Cancer Immunol Immunother (2014) 63:1213–1227
DOI 10.1007/s00262-014-1598-8

ORIGINAL ARTICLE

CpG-mediated modulation of MDSC contributes to the efficacy of Ad5-TRAIL therapy against renal cell carcinoma

Britnie R. James · Kristin G. Anderson · Erik L. Brincks · Tamara A. Kucaba · Lyse A. Norian · David Masopust · Thomas S. Griffith

Received: 3 April 2014 / Accepted: 7 August 2014 / Published online: 21 August 2014

Abstract Tumor progression occurs through the modulation of a number of physiological parameters, including the development of immunosuppressive mechanisms to prevent immune detection and response. Among these immune evasion mechanisms, the mobilization of myeloid-derived suppressor cells (MDSC) is a major contributor to the suppression of antitumor T-cell immunity. Patients with renal cell carcinoma (RCC) show increased MDSC, and methods are being explored clinically to reduce the prevalence of MDSC and/or inhibit their function. In the present study, we investigated the relationship between MDSC and the therapeutic potential of a TRAIL-encoding recombinant adenovirus (Ad5-TRAIL) in combination with CpG-containing oligodeoxynucleotides (Ad5-TRAIL/CpG) in an orthotopic mouse model of RCC. This immunotherapy effectively clears renal (Renca) tumors and enhances survival, despite the presence of a high frequency of MDSC in the spleens and primary tumor-bearing kidneys at the time of treatment. Subsequent analyses revealed that the CpG component of the immunotherapy was responsible for decreasing the frequency of MDSC in Renca-bearing mice; further, treatment with CpG modulated the phenotype and function of MDSC that remained after immunotherapy and correlated with an increased T-cell response. Interestingly, the CpG-dependent alterations in MDSC frequency and function did not occur in tumor-bearing mice complicated with diet-induced obesity. Collectively, these data suggest that in addition to its adjuvant properties, CpG also enhances antitumor responses by altering the number and function of MDSC.

B. R. James · E. L. Brincks · T. A. Kucaba · T. S. Griffith (✉)
Department of Urology, University of Minnesota, 3-125 CCRB, 2231 6th St. SE, Minneapolis, MN 55455, USA
e-mail: tgriffit@umn.edu

B. R. James · K. G. Anderson · D. Masopust · T. S. Griffith
Microbiology, Immunology, and Cancer Biology Graduate Program, University of Minnesota, Minneapolis, MN 55455, USA

K. G. Anderson · D. Masopust
Department of Microbiology, University of Minnesota, Minneapolis, MN 55455, USA

L. A. Norian
Department of Urology, The University of Iowa Carver College of Medicine, Iowa City, IA 52242, USA

L. A. Norian
Interdisciplinary Graduate Program in Immunology, The University of Iowa Carver College of Medicine, Iowa City, IA 52242, USA

L. A. Norian
Holden Comprehensive Cancer Center, The University of Iowa Carver College of Medicine, Iowa City, IA 52242, USA

L. A. Norian
Center for Immunology, The University of Iowa Carver College of Medicine, Iowa City, IA 52242, USA

D. Masopust · T. S. Griffith
Center for Immunology, University of Minnesota, Minneapolis, MN 55455, USA

T. S. Griffith
Masonic Cancer Center, University of Minnesota, Minneapolis, MN 55455, USA

Keywords TRAIL · MDSC · Immunotherapy · RCC · Diet-induced obesity

Abbreviations

5-FU	5-Fluorouracil
Ad5-TRAIL	Recombinant adenovirus encoding TRAIL
Ag	Antigen
Batf3	Basic leucine zipper transcription factor, ATF-like 3
BV650	Brilliant violet 650
CpG	CpG-containing oligodeoxynucleotide
DIO	Diet-induced obesity
HBSS	Hank's balanced salt solution
HFF	High-fat feed
IFN	Interferon
IL	Interleukin
i.p.	Intraperitoneal
IR	Intrarenal
i.v.	Intravascular
mAb	Monoclonal antibody
MACS	Magnet-associated cell sorting
MDSC	Myeloid-derived suppressor cell
MHC	Major histocompatibility complex
PBS	Phosphate-buffered saline
pDC	Plasmacytoid dendritic cell
PE	Phycoerytherin
pfu	Plaque-forming units
RCC	Renal cell carcinoma
spDC	Splenic dendritic cells
TCR	T-cell receptor
TLR	Toll-like receptor
TNF	Tumor necrosis factor
TRAIL	TNF-related apoptosis-inducing ligand
WT	Wild type

Introduction

The limited success of cancer immunotherapies can be attributed (in part) to the existence of immune escape strategies exerted by the tumor [1, 2], including MHC modulation, antigen sequestration, and immunosuppressive cytokine production [3]. Tumors also promote the recruitment and survival of regulatory cells that suppress effector cell responses. There has been considerable interest regarding the mobilization and recruitment of immunosuppressive myeloid-derived suppressor cells (MDSC) to sites of tumor growth [4, 5]. In these contexts, MDSC accumulate rapidly during primary tumor growth and directly influence antitumor immunity by suppressing effector T cells directly or indirectly via the increased production of immunosuppressive compounds like IL-10, TGF-β, arginase, and iNOS [6–8]. In recent years, investigation into improving the efficacy of tumor immunotherapy has utilized combinations of chemotherapeutics, small-molecule inhibitors, and radiation to overcome MDSC-mediated immunosuppression [9–11]. For example, metastatic renal cell carcinoma (RCC) patients have increased frequencies of MDSC in the peripheral blood, and current therapies for RCC (e.g., sunitinib) can reduce MDSC-mediated immune suppression [8, 11, 12]. It is posited that eliminating or modulating MDSC will restore the ability of immunotherapy to induce antitumor immunity; however, many treatments that target MDSC can have pleiotropic effects on other immune system components. For example, depletion of MDSC in mice using anti-Gr1 mAb [13] also depletes activated CD8 T cells [14] and plasmacytoid DC [15]. Chemotherapies such as 5-fluorouracil (5-FU), which can selectively eliminate MDSC at low doses [16], can have profound negative effects on the immune system [17, 18] potentially rendering immunotherapies ineffective.

Previous work from our laboratory described the use of a replication-deficient adenovirus encoding TNF-related apoptosis-inducing ligand (Ad5-TRAIL) [19] in combination with immunostimulatory CpG-containing oligodeoxynucleotides (CpG) for the treatment for metastatic RCC in mice [20]. Given that MDSC induced by tumors inhibit CD8 T-cell responses, we hypothesized that modulation of the number and/or function of MDSC after Ad5-TRAIL/CpG administration contributed to the overall success of this tumor immunotherapy. We found that CpG, alone or in combination with Ad5-TRAIL, altered MDSC frequency and function. Using a novel in vivo staining technique to discriminate cells located in tumor tissue from those in the vasculature [21], we found that Ad5-TRAIL/CpG significantly decreased the presence of MDSC specifically within the tissue of the tumor microenvironment, which correlated with an increase in activated CD8 T-cell accumulation in the tumor. Interestingly, when we examined responses in a model of diet-induced obesity (DIO), Renca-bearing obese mice had more MDSC than age-matched lean controls, and CpG treatment for obese mice failed to modulate MDSC frequency and function. Collectively, these data suggest that the efficacy of Ad5-TRAIL/CpG immunotherapy is enhanced by the ability of CpG to alter MDSC frequency and function, which allows the induced antitumor T-cell response to eliminate any residual tumor. The implications of these data are discussed.

Materials and methods

Animals and diets

Female wild-type BALB/c mice (7- to 8 week olds) were purchased from the National Cancer Institute (Frederick,

MD). For DIO studies, mice were given either standard chow or high-fat feed (HFF; Research Diets #12492, 60 % kcal from fat [22]). After 20 weeks, HFF mice were defined as obese if their body weight was >3 SD above the mean of mice fed standard chow ("lean"). All animal procedures were approved by the Institutional Animal Care and Use Committee at The University of Minnesota.

Cell lines and tumor challenge

The murine renal adenocarcinoma cell line, Renca [23], was obtained from Dr. Robert Wiltrout (National Cancer Institute, Frederick, MD) and was authenticated in 2010 by microsatellite marker analysis (Research Animal Diagnostic Laboratory, Columbia, MO). Renca cells were maintained in RPMI supplemented with 10 % fetal bovine serum, penicillin, streptomycin, sodium pyruvate, nonessential amino acids, 2-mercaptoethanol, and HEPES (hereafter referred to as complete RPMI), as previously described [20].

Intrarenal (IR) tumor challenge was performed as previously described [20, 22], where 2×10^5 Renca cells were injected into the left kidney. In some cases, mice were depleted of MDSC with anti-Gr1 mAb (1 mg i.p.) on day 6 after tumor implantation. On day 7, mice were injected in the tumor-bearing kidney with sterile PBS alone, Ad5-TRAIL (10^9 pfu) [24], and/or the non-methylated CpG ODN 1826 (5′-TCCATGACGTTCCTGACGTT-3′, 100 μg; IDT, Coralville, IA).

Immunofluorescent imaging

Immunofluorescent imaging was performed as previously described [21]. Briefly, tumor-bearing and contralateral kidneys were harvested 12 days after tumor implantation. Tissues were snap-frozen in OCT, cut into 7-μm thickness, and fixed in acetone for 10 min. Sections were stained using unconjugated rabbit anti-cytokeratin 8 (NB100-91850) and 18 (NBP1-67610; Novus Biologics; Littleton, CO), AF488-conjugated donkey anti-rabbit secondary Ab (Jackson ImmunoResearch Laboratories; West Grove, PA), PE-conjugated anti-CD31 (MEC13.3; eBioscience), BV421-conjugated anti-CD11b (M1/70; BioLegend), and APC-conjugated anti-Gr-1 mAb (RB6.8C5; eBioscience) and imaged with a Leica DM5500 B microscope.

Flow cytometry

Single-cell suspensions of tumor-bearing or contralateral kidneys and spleens were prepared using a gentleMACS Dissociator (Miltenyi BioTeck Inc., Auburn, CA) and then digested for 15–30 min in HBSS containing 0.56 Wuensch units/ml of Liberase Blendzyme 3 (Roche, Branford, CT) and 0.15 mg/ml DNAse I (Sigma, St. Louis, MO). After blocking with a cocktail of anti-CD16/32 and normal mouse serum, cells were stained with combinations of the following mAb [eBioscience (San Diego, CA) or BioLegend (San Diego, CA)] and analyzed using multi-parameter flow cytometry on a BD LSR II (BD Biosciences, San Diego, CA) and FlowJo software (TreeStar Inc., Ashland, OR): MDSC—anti-CD3-, CD11c-, CD19-PE, or PerCP/Cy5.5 (dump gate), CD11b-PE/Cy7, Ly6C (HK1.1)-APC/Cy7, Ly6G (1A8)-FITC, I-A^d-PacBlue, CD40-PE, CD86-PE/Cy5, CD80-BV650; T cells—anti-CD3-PerCP/Cy5.5, CD4-PE/Cy7, CD8-PacBlue, CD44-PE or -AF700, CD45.2-PE, and -BV650. Intracellular staining for Foxp3 was done, as a dump gate, using a Foxp3 staining kit (eBioscience).

To identify leukocytes located in the tumor-bearing kidney tissue or kidney vasculature, intravascular (i.v.) staining was done as previously described [21, 25]. Briefly, tumor-bearing mice were injected with 3 μg of PE-conjugated anti-CD45.2 mAb i.v. 3 min before killing. Single-cell suspensions from organs were then processed for flow cytometric analyses as described above. Additionally, cells were stained ex vivo with BV650-conjugated anti-CD45.2 mAb. Duel staining of CD45.2 discriminates between cells within the vasculature (CD45.2-PE^+CD45.2-$BV650^+$) or tissue (CD45.2-PE^-CD45.2-$BV650^+$) at the time of harvest. Blood and inguinal lymph nodes served as positive and negative controls for i.v. staining, respectively.

MDSC enrichment and isolation

The MDSC from tumor-bearing kidneys were enriched using Miltenyi anti-CD11b microbeads and then sort-purified on a BD Aria II or FACS DiVa based on CD45.2^+/$CD11c^{low}$/$CD11b^+$/$Ly6C^+$/$Ly6G^{+/-}$ expression after gating on live cells via Hoechst 33258 exclusion. Sorted MDSC purity was ≥95 %. Alternatively, MDSC were purified by negative selection with Miltenyi anti-CD11c microbeads. Cells were run over two sequential columns, and the negative fractions were collected. $CD11c^-$-enriched cells were then incubated with Miltenyi anti-CD11b microbeads and run over two sequential columns, and the bound fractions were collected. MDSC purity was ≥90 % of live cells.

T-cell proliferation assay

The Ag-specific assay: T cells were harvested from naïve DUC18 TCR transgenic mice [26]. Splenic DC (spDC) from tumor-free BALB/c mice were isolated with Miltenyi anti-CD11c microbeads. T-cell proliferation was assessed by culturing naive DUC18 T cells (5×10^4 cells/well) with tERK peptide-pulsed spDC (5×10^3 cells/well) with increasing numbers of sort-purified splenic or renal MDSC from tumor-bearing mice in a flat-bottom 96-well plate.

[^{3}H] Thymidine was added during the final 18 h of a 72-h incubation. Relative T-cell proliferation was set to 100 % for control T-cell/DC cocultures not containing MDSC. The % relative proliferation was then calculated for all other culture conditions. Anti-CD3 assay: Naïve splenic BALB/c CD8 T cells and MDSC from tumor-bearing mice were MACS-purified as described above. When indicated, MDSC were stimulated with 6 μg CpG for 3 h and then

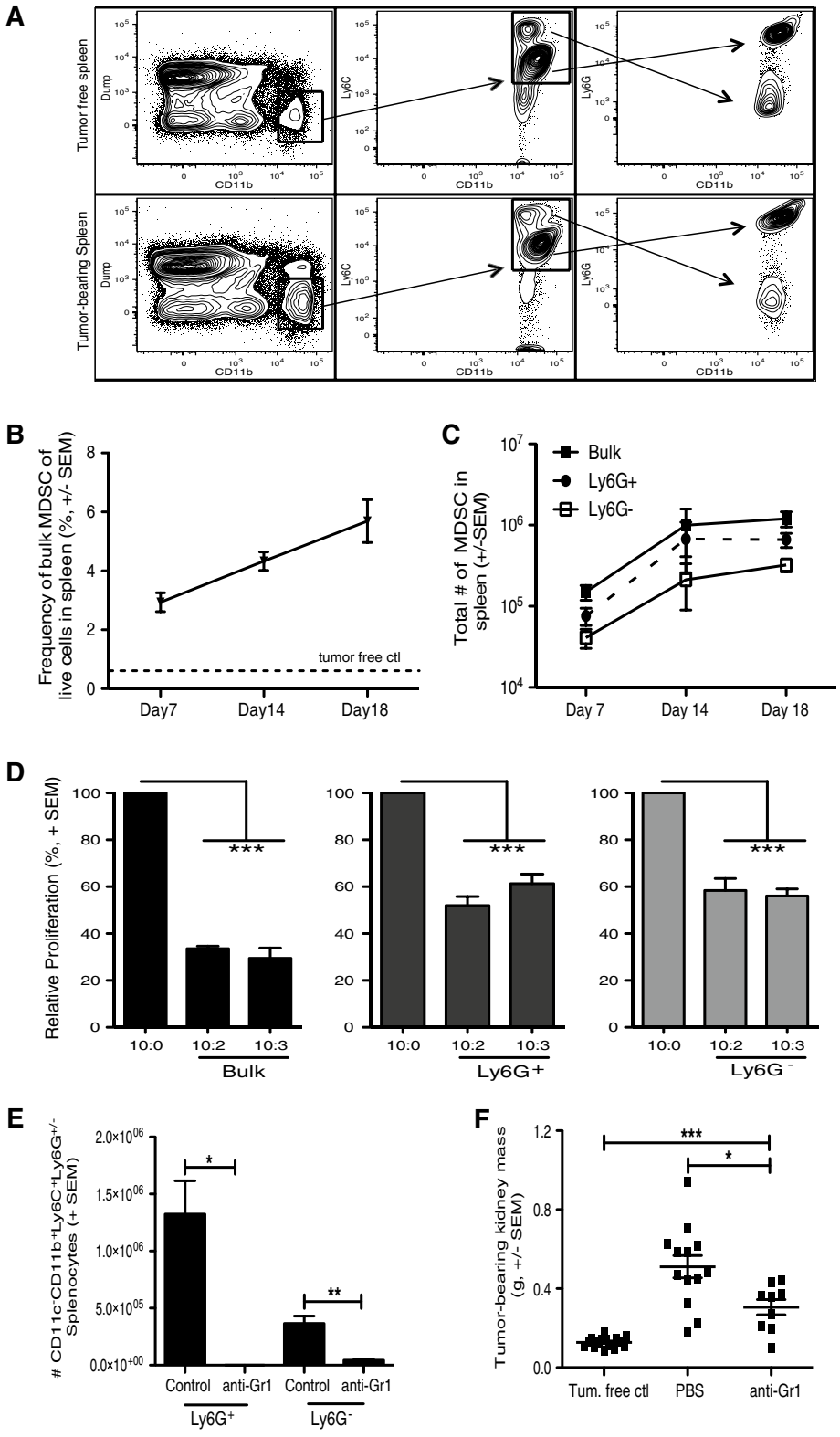

Fig. 1 Characterization of MDSC in spleens of Renca tumor-bearing mice. BALB/c mice were implanted IR with 2×10^5 Renca. **a–c** Spleens were harvested from tumor-bearing mice 7, 14, and 18 days post-tumor implantation. Single-cell suspensions were made, and cells were stained for flow cytometric analysis. **a** Representative flow plots showing the gating for bulk MDSC ($CD3^-CD19^-CD11c^-CD11b^+Ly6C^+$) and $Ly6G^+$ and $Ly6G^-$ MDSC subsets within spleens. Representative splenic data from a tumor-free mouse stained in the same manner are shown to demonstrate the tumor-induced increase in cells of this phenotype. **b**, **c** Mean (±SEM) frequency and number of bulk and subset MDSC in spleens during tumor challenge. Data are representative of three independent experiments, with at least 3 mice/group/experiment. For reference, the dashed line in B indicates the frequency of MDSC in tumor-free mice. **d** Spleens were harvested after 18–21 days. Bulk MDSC, $Ly6G^+$, and $Ly6G^-$ MDSC subsets were sort-purified to ≥95 % purity. MDSC were seeded in increasing numbers into DUC18 $CD8^+$ T cell and tERK-pulsed DC cocultures for 72 h. Cocultures were pulsed with [^{3}H] thymidine during the last 18 h of incubation to assess proliferation. Relative mean (±SEM) $CD8^+$ T-cell proliferation was calculated based on normalization to the 10 $CD8^+$ T cells/1 spDC/0 MDSC control group. Data are representative of two independent experiments, and samples were each run in triplicate. Cultures containing bulk MDSC were compared to the control group using 2-way ANOVA, $***p \leq 0.001$. **e** Mean (±SEM) number of $CD11c^-CD11b^+Ly6C^+Ly6G^{+/-}$ splenocytes in tumor-bearing mice given 1 dose of 1 mg control rat IgG or anti-Gr1 mAb. **f** Mean (±SEM) kidney weight (g) from tumor-bearing mice was determined on day 12. Data are representative of three independent experiments, with at least 5 mice/group/experiment. $*p \leq 0.05$, $**p \leq 0.01$, $***p \leq 0.001$ using Student's *t* test

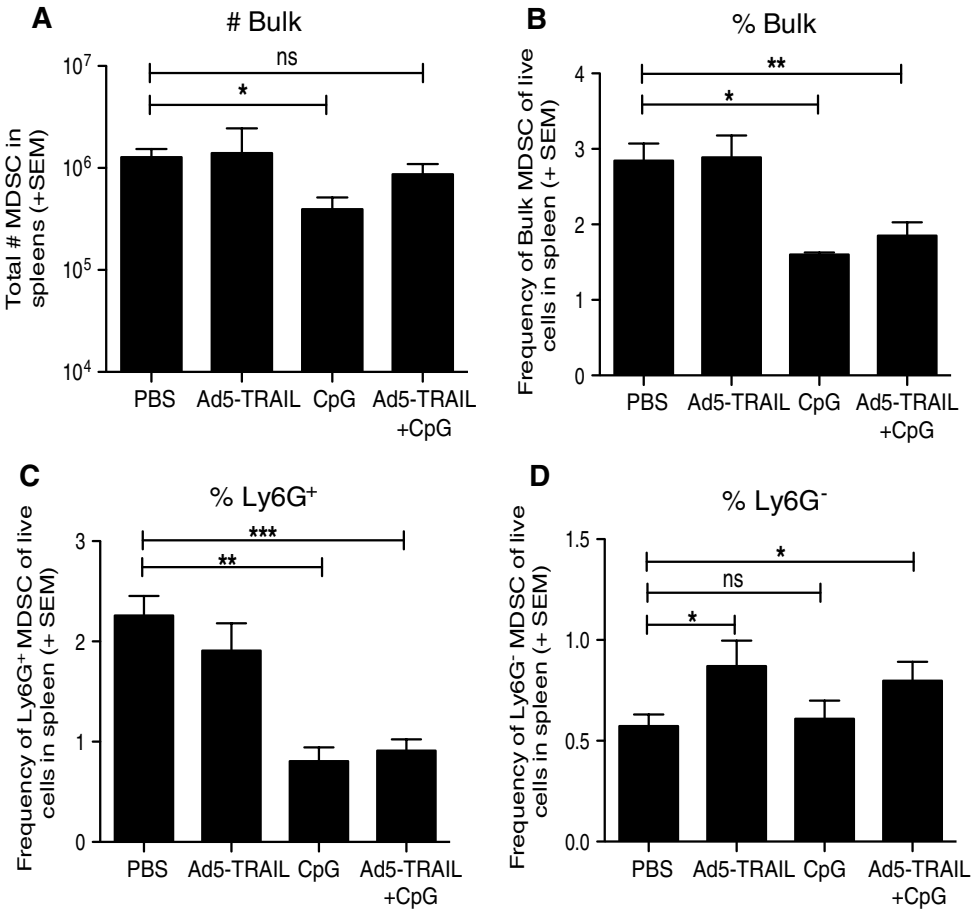

Fig. 2 CpG decreases MDSC in tumor-bearing mice. BALB/c mice were implanted IR with 2×10^5 Renca and treated with PBS, Ad5-TRAIL alone, CpG alone, or Ad5-TRAIL/CpG on day 7. Spleens were harvested on day 12 and processed for flow cytometry to determine the (**a**) number of bulk MDSC and (**b**–**d**) frequency of bulk, $Ly6G^+$, or $Ly6G^-$ $CD3^-CD19^-CD11c^-CD11b^+$ $Ly6C^+$ MDSC. Mean (±SEM) frequency of splenic MDSC from tumor-bearing mice is shown, and data are representative of four independent experiments with at least mice/group/experiment. For all experiments $^*p \leq 0.05$, $^{**}p \leq 0.01$, $^{***}p \leq 0.001$ using Student's *t* test

washed 3× with PBS. Wells of a round-bottom 96-well plate were coated with anti-CD3 mAb (clone 500A2; 1 μg/ml) overnight at 4 °C. The plate was then washed with PBS and CD8 T cells (5×10^4 cells per well), and increasing numbers of CpG-stimulated and CpG-unstimulated MDSC were plated. [^{3}H] Thymidine was added as above, and % relative proliferation was calculated.

Quantitative real-time PCR (qPCR)

Tumor-bearing kidneys were harvested 4 h after treatment and homogenized via gentleMACS Dissociator. Total RNA was isolated using TRIzol reagent (Invitrogen, Carlsbad, CA), and 1 μg was reverse-transcribed using Superscript III. Resulting cDNA was used as a template for qPCR using TaqMan primer/probe sets for *arg1* and 18 s rRNA (PE Applied Biosystems, Foster City, CA).

Statistical analysis

Statistical analysis between groups was determined by unpaired or paired Student's *t* test and 2-way ANOVA where appropriate. Data were analyzed with Prism4 GraphPad software, and statistical significance is indicated in figure legends [$^*p < 0.05$; $^{**}p < 0.001$; $^{***}p < 0.0001$; not significant (n. s.)].

Results

Characterization of splenic MDSC from RCC tumor-bearing mice

The Renca cell line is commonly used to model RCC in mice, where it can be injected subcutaneously to produce localized tumors or intravenously to produce experimental lung metastases [6, 24, 27, 28]. In contrast, we use an orthotopic model, similar to the model described by Salup et al. [29], where direct implantation of Renca cells into the kidney leads to the formation of an aggressive primary IR tumor as well as lung metastases [20]. Investigation of MDSC in mice bearing Renca tumors has been limited, so we initially characterized the MDSC present in mice bearing such orthotopic Renca tumors. MDSC are identified by CD11b with the concomitant expression of Ly6C and Ly6G [30], and accumulate in Renca-bearing mice compared to tumor-free mice (Fig. 1a). Differential Ly6G expression defines granulocytic and monocytic MDSC, respectively,

which can suppress T cells by distinct mechanisms [31]. Assessment of MDSC population dynamics after tumor implantation revealed a steady increase in the frequency and number of bulk ($CD3^-CD19^-CD11c^{low}CD11b^+Ly6C^+$) MDSC in the spleen over time (Fig. 1b, c). Of note, both the $Ly6G^+$ granulocytic ($CD3^-CD19^-CD11c^{low}CD11b^+Ly6C^+Ly6G^+$) and $Ly6G^-$ monocytic ($CD3^-CD19^-CD11c^{low}CD11b^+Ly6C^+Ly6G^-$) MDSC populations expanded similarly in the spleen over time. To verify that the MDSC phenotype correlated with suppressive function by these populations, splenic MDSC were isolated from Renca-bearing mice and cocultured with CD8 T cells [32]. Indeed, Ag-specific T-cell proliferation was significantly suppressed when either bulk, $Ly6G^+$, or $Ly6G^-$ MDSC were included in the assay (Fig. 1d). To assess the extent to which Renca-mobilized MDSC supported tumor growth, we employed the common MDSC depletion method of administering anti-Gr1 mAb (Fig. 1e) in our RCC tumor-bearing mice and assessed tumor burden. Depletion of MDSC significantly decreased tumor burden (Fig. 1f), suggesting that the MDSC mobilized as a result of a growing Renca tumor indeed support tumor growth.

CpG decreases MDSC and alters MDSC subtype distribution

Having previously described the ability of Ad5-TRAIL/CpG therapy to induce effective systemic antitumor immunity, we were interested in determining how Ad5-TRAIL/CpG was efficacious against Renca tumors in the face of an enhanced population of MDSC. The data in Fig. 1 demonstrated the accumulation of immunosuppressive MDSC in RCC tumor-bearing mice, leading us to hypothesize that Ad5-TRAIL/CpG therapy must modulate MDSC systemically and locally to permit the generation of an antitumor T-cell response capable of clearing the primary tumor within the kidney. To determine the extent to which Ad5-TRAIL/CpG therapy altered the number of MDSC in tumor-bearing mice, BALB/c mice were implanted IR with Renca cells and treated with PBS, Ad5-TRAIL, and/or CpG on day 7. Analysis of bulk splenic MDSC on day 12 found that Ad5-TRAIL alone or in combination with CpG did not modulate the MDSC population, but CpG alone significantly decreased the number of bulk MDSC (Fig. 2a). However, consistent with the previous data [20], mice that received CpG (with or without Ad5-TRAIL) were presented with splenomegaly resulting in increased total splenocytes counts. Because increased cell numbers in treatment groups can mask effects the treatment may have on cell distribution (frequency), we also determined MDSC frequency within spleens of PBS, CpG-, and/or Ad5-TRAIL-treated tumor-bearing mice. We found that CpG alone or in combination with Ad5-TRAIL significantly decreased the frequency of the bulk MDSC population (Fig. 2b). We extended this analysis to examine the $Ly6G^+$ and $Ly6G^-$ MDSC populations and found that the $Ly6G^+$ MDSC experienced a similar decrease after administration of CpG alone or in combination with Ad5-TRAIL (Fig. 2c). Interestingly, the frequency of $Ly6G^-$ MDSC significantly increased in the spleen after injection of Ad5-TRAIL (alone or with CpG; Fig. 2d), but the frequency of this MDSC population was much lower (<1 %) than the other populations examined suggesting that this statistical change likely has minimal biological impact. Together, these data suggest that local administration of CpG into tumor-bearing kidneys systemically modulates the frequency of MDSC in Renca-bearing mice.

Fig. 3 Characterization of MDSC within tumor-bearing kidneys. ▶ BALB/c mice were implanted IR with 2×10^5 Renca. **a** WT tumor-bearing kidneys were harvested on day 12 for IF imaging to identify MDSC. *i*, *ii* 10× images were taken and stitched together to view the entire tumor-bearing kidney, and tumor margin architecture with CD31 and cytokeratins 8 and 18. The tumor margin image also includes Gr-1 and CD11b staining to visualize MDSC. *iii* Separate 20× images were taken to visualize Gr-1 alone, CD11b alone, and merged $Gr\text{-}1^+CD11b^+$ cells within the tumor using the structural markers to identify the regions of tumor tissue and vasculature within the kidney. Images are representative of four independent experiments totaling 8 mice. **b** Tumor-bearing and contralateral kidneys were harvested from mice 7, 14, or 18 days post-tumor implantation. Single-cell suspensions were made, and cells were stained for flow cytometric analysis. Mean (±SEM) frequency and number of bulk, $Ly6G^+$, or $Ly6G^-$ MDSC in tumor-bearing kidneys during tumor challenge. Data are representative of three independent experiments, with at least 3 mice/group/experiment. **c** Tumor-bearing kidneys were harvested after 18–21 days. Bulk MDSC were sort-purified to ≥95 % purity. Cocultures were plated and pulsed with $[^3H]$ thymidine during the last 18 h of incubation to assess proliferation. Relative mean (±SEM) $CD8^+$ T-cell proliferation was calculated based on normalization to the 10 $CD8^+$ T cells/1 spDC/0 MDSC control group. Data are representative of two independent experiments where samples were each run in triplicate. Cultures containing bulk MDSC were compared to the control group using 2-way ANOVA, $^{***}p \leq 0.001$

Ad5-TRAIL/CpG alters the location of MDSC within the tumor-bearing kidney

Data suggest MDSC acquire their suppressive function only after exposure to factors in the tumor microenvironment [33, 34]. Moreover, MDSC within the tumor might have the greatest effect on antitumor T-cell responses [35]. Consequently, we examined the impact of Ad5-TRAIL/CpG therapy on the MDSC in the tumor-bearing kidney, in addition to the MDSC in the spleen of tumor-bearing mice. To this end, we first examined the presence and location of MDSC in Renca tumor-bearing kidneys by immunofluorescence. Structural markers for vasculature (CD31) and tumor (cytokeratins 8 and 18 [36]) were used to visualize the tumor-bearing kidney (Fig. 3Ai). The MDSC markers CD11b and Gr1 were used to examine MDSC location

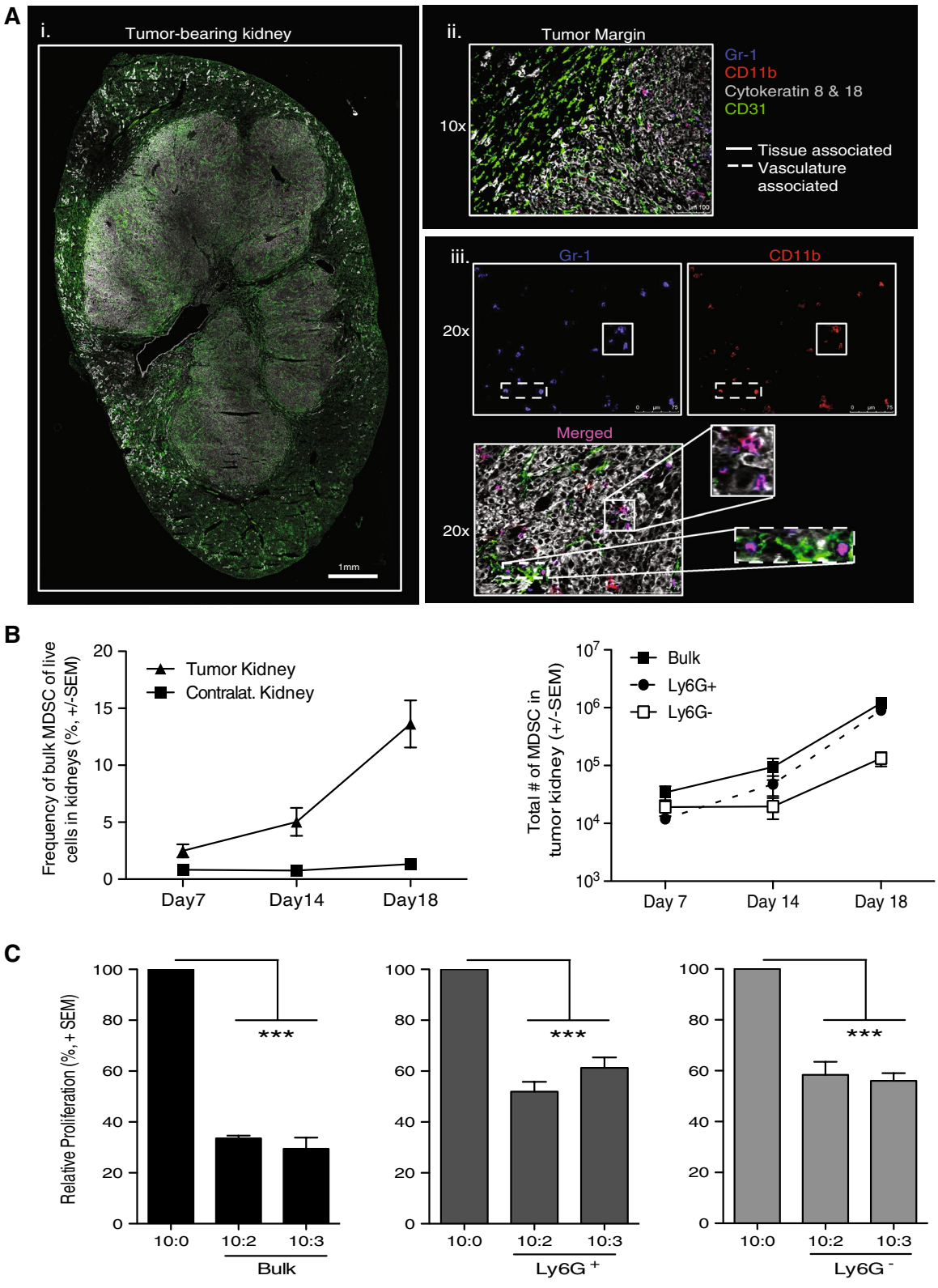

in the tumor-bearing kidney. When examining the tumor margin, MDSC were primarily localized within the tumor and not in the "normal" tissue of the kidney (Fig. 3Aii). Further, MDSC were associated with both tumor tissue and vasculature, as seen by colocalization with cytokeratin 8 and 18^{+} and CD31^{+} cells, respectively (Fig. 3Aiii). Subsequent analysis of MDSC within tumor-bearing and contralateral kidneys by flow cytometry demonstrated

MDSC accumulation only within the tumor-bearing kidney (Fig. 3b), and both bulk MDSC and the individual subsets of MDSC isolated from tumor-bearing kidneys had the capacity to suppress T-cell proliferation (Fig. 3c), similar to the splenic MDSC in this model.

Kidneys are highly vascular organs, making it likely that flow cytometric evaluation of MDSC from tumor-bearing kidneys would include both "tissue-localized" MDSC and MDSC present in the vasculature at the time of organ harvest. To clearly distinguish MDSC within the kidney tissue from MDSC within the vasculature, we used an intravascular staining technique [21, 25] in which PE-labeled anti-CD45.2 mAb was injected i.v. prior to tumor-bearing kidney harvest. Tumor-bearing and contralateral kidneys were then processed for flow cytometry, which included ex vivo staining with BV650-labeled anti-CD45.2 mAb. Using this method, leukocytes in the vasculature at the time of harvest stained positive with both the PE- and BV650-labeled anti-CD45.2 mAb, whereas leukocytes truly within the kidney tissue were only stained by the ex vivo BV650-labeled anti-CD45.2 mAb (Fig. 4a). This technique is superior to perfusion as a substantial number of cells remain in the vasculature after perfusion, and the increased vasculature pressure that occurs during perfusion can disrupt tissue architecture [21]. When gating on the location (kidney tissue vs. vasculature) of the cells, the number of MDSC were evenly distributed between the vasculature and the tissue (Fig. 4b). Within the tissue specifically, ~15 % of the $CD45.2^+$ cells ("CD45.2 i.v. negative") were $Ly6G^+$ MDSC and only ~7 % were $Ly6G^-$ MDSC (Fig. 4b). Analysis of contralateral kidneys showed that the majority of MDSC were in the vasculature (Fig. 4c). Immunofluorescence microscopy verified that "CD45.2 i.v. positive" cells were located within vascular endothelium or glomerular regions of the kidney (data not shown).

Having established the utility of this intravascular staining technique to identify and quantitate the MDSC truly within the tissue of tumor-bearing kidneys, we then used this method to examine the effect of Ad5-TRAIL/CpG therapy on MDSC localization. Similar to the analyses of the whole tumor-bearing kidney that would include both tissue- and vasculature-localized cells, Ad5-TRAIL/CpG therapy decreased the number and frequency of bulk MDSC in the kidney tissue, as well as the frequency of $Ly6G^+$ MDSC (Fig. 4d). Though the frequency of $Ly6G^-$ MDSC was not significantly decreased in the kidney tissue, there was a trend toward a decrease (Fig. 4d). Importantly, the frequency of MDSC within the kidney vasculature was not altered by Ad5-TRAIL/CpG administration (Fig. 4e). These data collectively demonstrate that Ad5-TRAIL/CpG therapy decreases the number and frequency of MDSC specifically within the kidney tissue.

Fig. 4 Ad5-TRAIL/CpG therapy alters MDSC location within the tumor-bearing kidney. BALB/c mice were implanted IR with 2×10^5 Renca cells and treated with PBS or Ad5-TRAIL/CpG on day 7 (some mice received no injection). Tumor-bearing and contralateral kidneys were harvested on day 12. Prior to harvest, all mice were injected i.v. with PE-conjugated anti-CD45.2 mAb (3 μg) in PBS to discriminate tissue- from vasculature-associated MDSC, and killed 3 min later. Single-cell suspensions of tumor-bearing kidneys were prepared and stained for flow cytometric analyses to assess MDSC cell infiltration. **a** Representative flow plots for tissue- or vasculature-localized MDSC in tumor-bearing and contralateral kidneys from untreated mice. **b**, **c** Mean (±SEM) number and frequency of tissue- and vasculature-localized MDSC from (**b**) tumor-bearing or (**c**) contralateral kidneys. Data are representative of three independent experiments totaling 8 mice. **d**, **e** Mean (±SEM) number and frequency of bulk MDSC, $Ly6G^+$, or $Ly6G^-$ MDSC in the tissue (**d**) and vasculature (**e**) of tumor-bearing kidneys from mice treated with either PBS or Ad5-TRAIL/CpG on day 7. Data are representative of four independent experiments with at least 4 mice/group/experiment. For all experiments $^{**}p \leq 0.01$, $^{***}p \leq 0.001$, *n.s.* not significant using Student's *t* test

CpG alters MDSC phenotype and function

While modulating MDSC numbers can improve the efficacy of therapy, altering MDSC function can also ablate their inhibitory capacity to improve therapeutic outcomes. Consequently, much of the current research targeting MDSC is aimed at both decreasing their frequency and reducing their inhibitory capacity. To determine the extent to which CpG may also be affecting the functionality of MDSC, we performed a series of in vitro and in vivo analyses of MDSC from spleens and kidneys of Renca-bearing mice. BALB/c mice were implanted with Renca tumors, and spleens and tumor-bearing kidneys were harvested 18–21 days later to allow for increased MDSC numbers. MDSC were enriched from both spleens and tumor-bearing kidneys, and then stimulated in vitro with CpG overnight. The CpG-stimulated MDSC exhibited a "matured" phenotype, based on increased CD40, CD80, CD86, and MHC II expression when compared to unstimulated MDSC from spleens (Fig. 5a) and kidneys (data not shown), suggesting a direct effect of CpG on the MDSC population. Next, we determined the extent to which CpG stimulation affected the suppressive capacity of the MDSC. MDSC purified from tumor-bearing kidneys were stimulated with CpG for 3 h. After washing to remove any CpG from the culture, the CpG-stimulated MDSC were then added into cultures of anti-CD3 mAb-stimulated CD8 T cells to assess their ability to suppress T-cell proliferation. Compared to unstimulated MDSC, the CpG-stimulated MDSC were less suppressive of T-cell proliferation (Fig. 5b). These data are consistent with the idea that CpG can directly stimulate MDSC [37].

We extended the analysis in vivo to see the extent to which CpG administration changed MDSC within the tumor-bearing kidney. Renca-bearing mice were injected

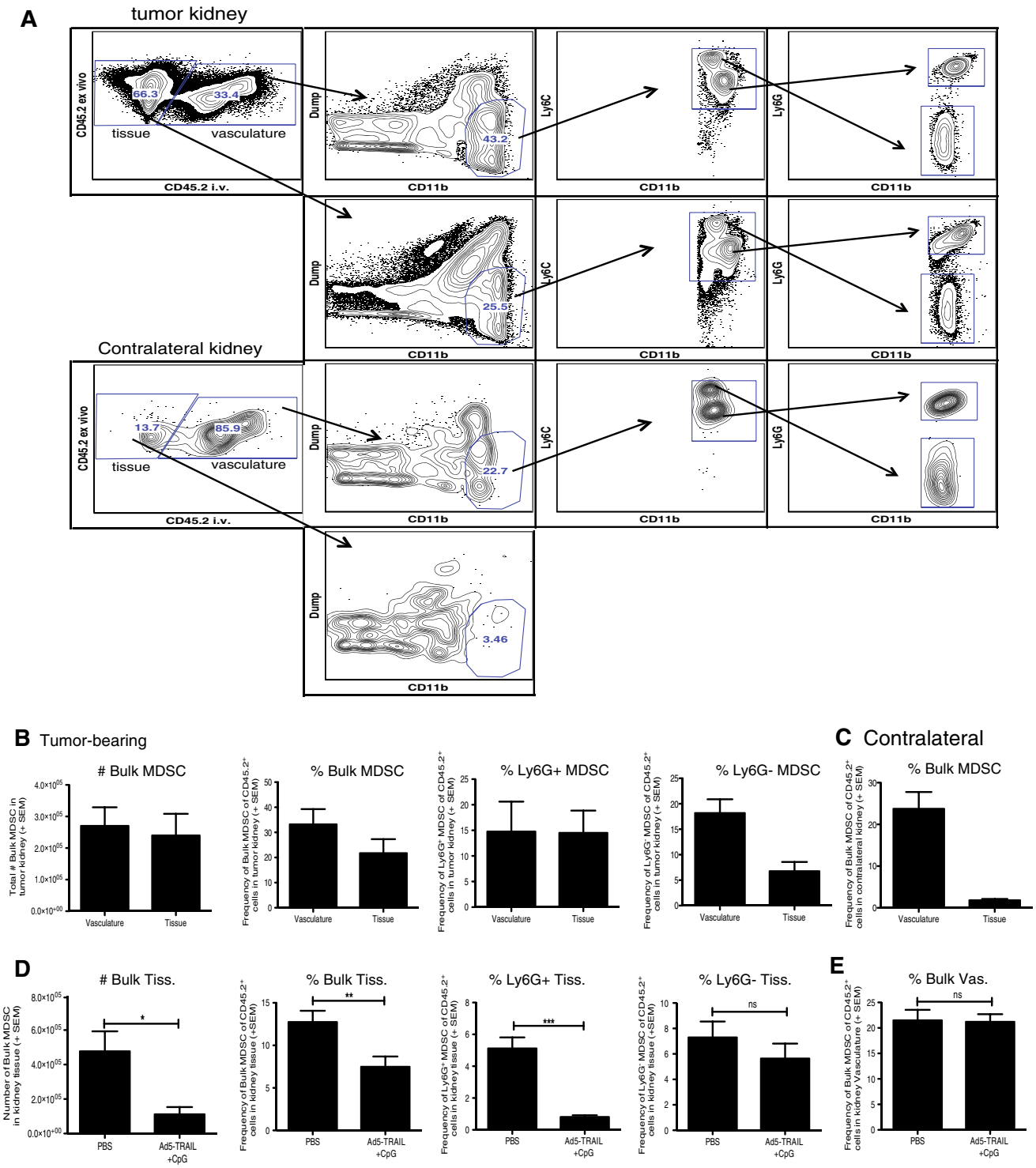

with PBS or CpG intrarenally on day 7, and the kidneys were harvested 4 h or 5 days later and processed for qPCR analysis or flow cytometric analysis of the MDSC, respectively. Seeing the reduction in suppressive capacity in Fig. 5b, we examined the expression of mRNA for arginase 1 (*arg1*), an enzyme utilized by MDSC to suppress T-cell proliferation [8], within tumor-bearing kidneys after PBS or CpG injection. When normalized to tumor-free kidneys, the amount of *arg1* mRNA was significantly reduced after CpG administration (Fig. 5c). These data, when coupled with the data in Fig. 5b, suggest CpG can rapidly and inherently alter MDSC. When we examined the phenotype of MDSC, there were increased frequencies of $CD40^{hi}$, $CD86^{hi}$, or MHC II^{hi} MDSC from mice injected with CpG

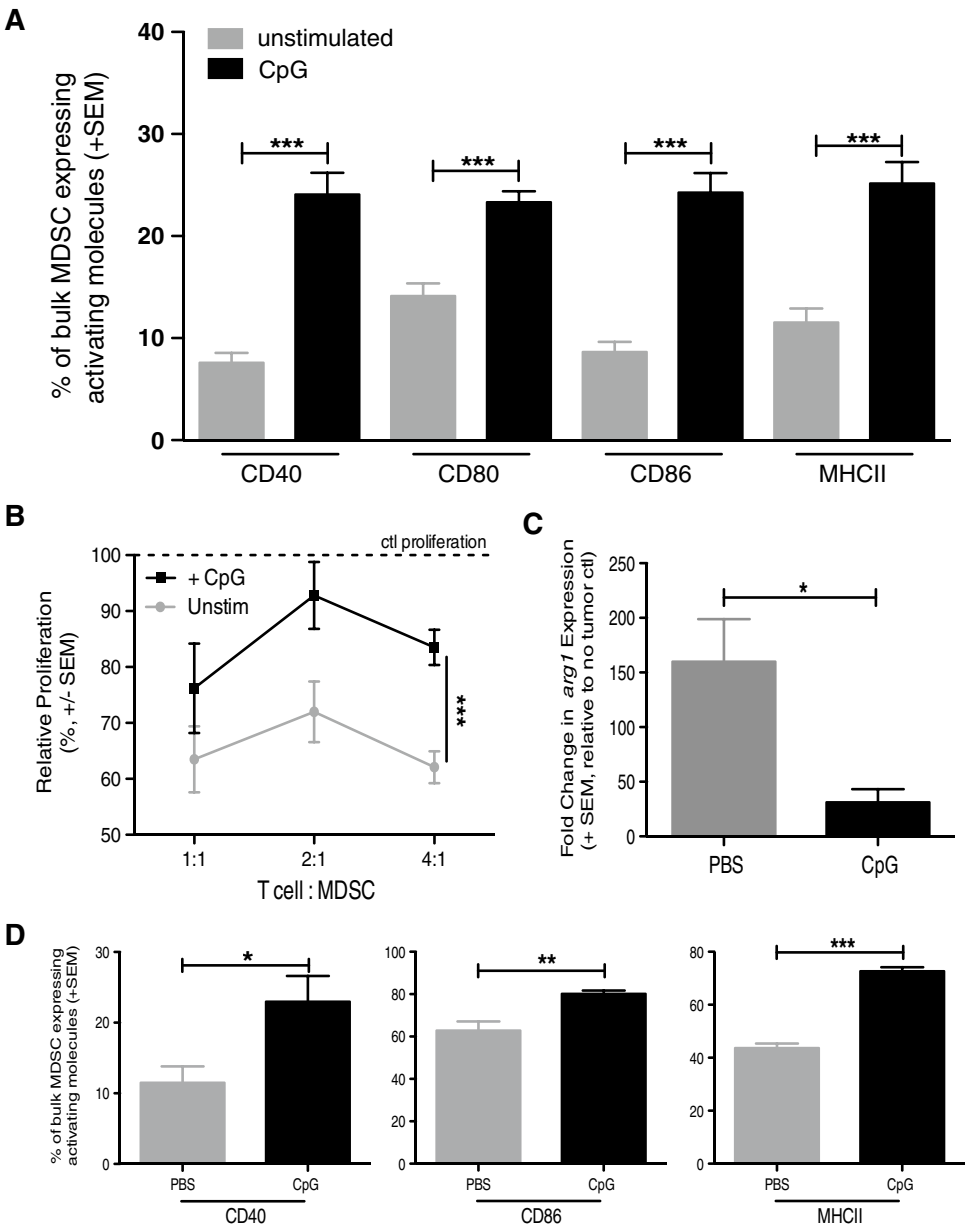

Fig. 5 CpG alters MDSC phenotype and function in vitro and in vivo. BALB/c mice were implanted IR with 2×10^5 Renca, and tumor-bearing kidneys and spleens were harvested days 18–21. **a** Splenocytes were plated at 10^6 cells/well in a 24-well plate. Cells were either treated with 100U of IFN-γ or 6 μg CpG overnight. Cells were harvested from plate and stained for flow cytometric analysis. **a** Mean (±SEM) frequency of $CD3^-CD19^-CD11c^-CD11b^+Ly6C^+$ MDSC expressing high levels of CD40, CD80, CD86, MHC II. Data are representative of three independent experiments with at least 4 mice/group/experiment. **b** Mean (±SEM) proliferation of naïve WT BALB/c splenic $CD8^+$ T cells stimulated with 1 μg/ml anti-CD3 mAb and cocultured with CpG-stimulated bulk MDSC. Ratios represent #$CD8^+$ T cells: #MDSC. Cocultures were pulsed with [^{3}H] thymidine during the last 18 h of incubation to assess proliferation. Data are representative of two independent experiments in which samples were each run in triplicate, $^{***}p \leq 0.001$ using 2-way ANOVA. **c** qPCR analysis of *arg1* expression in Renca-bearing kidneys 4 h after injection of PBS or CpG. **d** BALB/c mice were implanted IR with 2×10^5 Renca and treated with CpG alone or PBS on day 7, and tumor-bearing kidneys were harvested day 12. Single-cell suspensions were made and stained for flow cytometric analysis. Mean (±SEM) frequency of MDSC expressing high levels of CD40, CD86, and MHC II. Data are representative of two independent experiments with at least 4 mice/group/experiment. For all experiments (except where noted), $^*p \leq 0.05$, $^{**}p \leq 0.01$, $^{***}p \leq 0.001$ using Student's *t* test

compared to PBS-injected mice (Fig. 5d), similar to the in vitro data in Fig. 5a. Thus, the data in Fig. 5 suggest that CpG can have direct effects on MDSC in vitro and induce inherent changes in vivo.

Diet-induced obese tumor-bearing mice have increased MDSC frequencies that are not affected by CpG

The number and suppressive function of MDSC increase with inflammation [38]. There are a variety of clinical settings marked by increased and/or chronic inflammation, and obesity is one such condition in which chronic inflammation and the increased production of pro-inflammatory cytokines and adipokines promote immune system dysfunction [39]. We recently described how Ad5-TRAIL/CpG therapy is ineffective in clearing Renca tumors in diet-induced obese (DIO) mice [22]. Because obesity can induce significant MDSC accumulation and activation in the absence of tumors [40], we hypothesized that one explanation for the ineffectiveness of Ad5-TRAIL/CpG therapy in DIO Renca-bearing mice was exacerbated MDSC accumulation that was not modulated by CpG. Thus, we examined the frequency of MDSC in the spleens and tumor-bearing kidneys from DIO mice and age-matched mice fed standard chow ("lean" mice). There was a significant increase in the frequency of bulk and $Ly6G^+$ MDSC in the spleens (Fig. 6a) and bulk, $Ly6G^+$, and $Ly6G^-$ MDSC in tumor-bearing kidneys (Fig. 6b) from DIO mice compared to lean mice. Utilizing

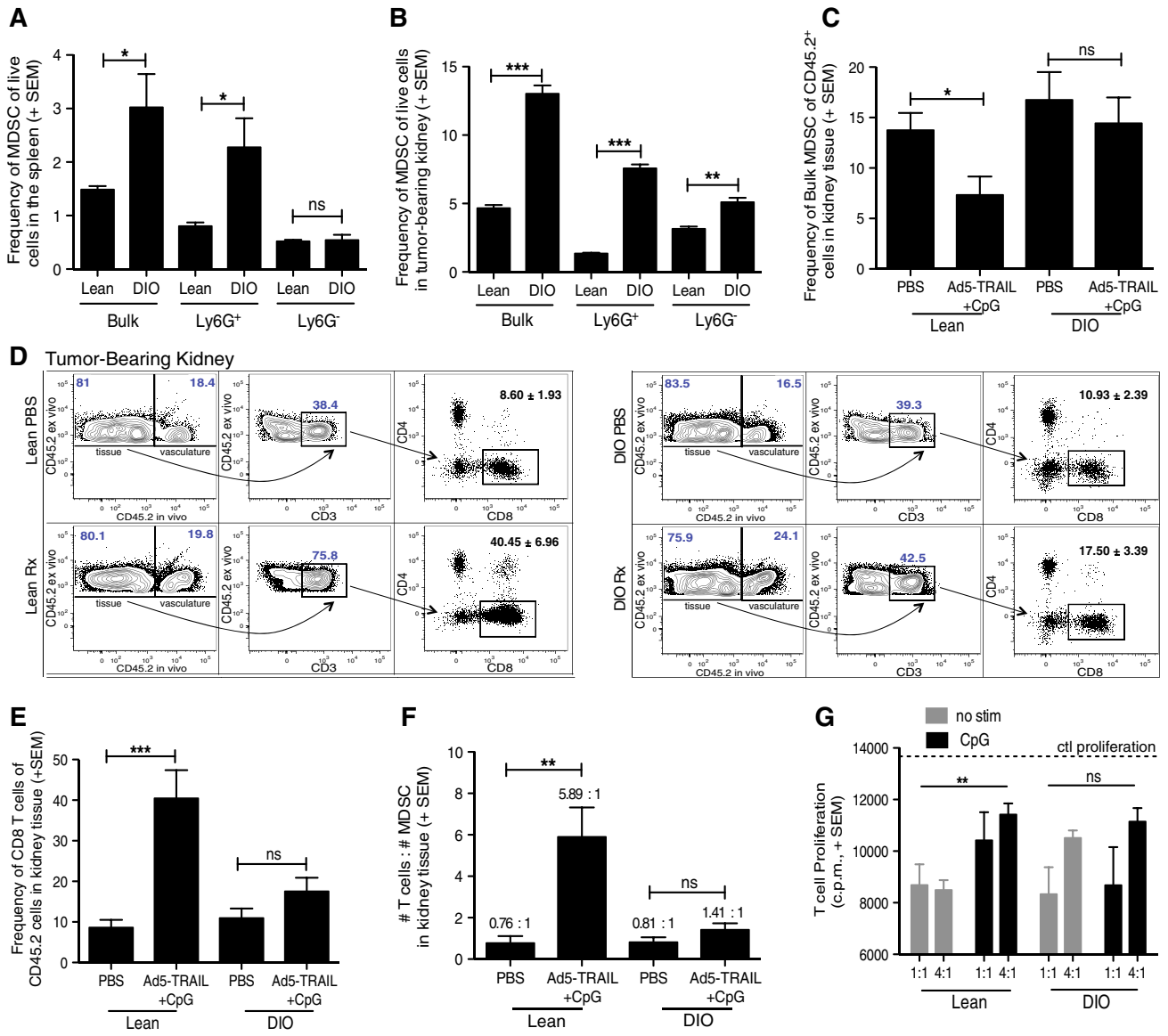

Fig. 6 DIO tumor-bearing mice have increased MDSC that do not respond to CpG resulting in a diminished antitumor response. Lean and DIO BALB/c mice were implanted IR with 2×10^5 Renca cells on day 0 and either left untreated (**a**, **b**), or treated with PBS or Ad5-TRAIL/CpG on day 7 (**c**–**f**). Spleens and tumor-bearing kidneys were harvested day 12, homogenized, and single-cell suspensions were made and stained for flow cytometric analyses. Mean (±SEM) frequency of MDSC in **a** spleens and **b** tumor-bearing kidneys. **c**–**f** Mean (±SEM) frequency, using i.v. staining, of **c** MDSC, **d**–**e** $CD8^+$ T cells, and **f** ratio of the number of $CD8^+$ T cells to the number of MDSC. Data are representative of two independent experiments with at least 4 mice/group/experiment. For all experiments, $*p \leq 0.05$, $**p \leq 0.01$, $***p \leq 0.001$ using Student's *t* test. **g** Mean (±SEM) $CD8^+$ T-cell proliferation from MACS-purified naïve WT BALB/c splenic $CD8^+$ T cells stimulated with 1 μg/ml anti-CD3 mAb and cocultured with CpG-stimulated MACS-purified bulk MDSC from either lean or DIO tumor-bearing kidneys. Ratios represent #$CD8^+$ T cells: #MDSC. Cocultures were pulsed with [^{3}H] thymidine during the last 18 h of incubation to assess proliferation. Data are representative of two independent experiments in which samples were each run in triplicate, $***p \leq 0.001$ using 2-way ANOVA

the in vivo staining technique described in Fig. 4, we examined the frequency of MDSC specifically within the tumor-bearing kidney tissue from lean and DIO mice that had been treated with either PBS or Ad5-TRAIL/CpG. In contrast to MDSC from lean mice, the MDSC frequency in the tumor-bearing kidneys of DIO mice did not significantly change after Ad5-TRAIL/CpG therapy (Fig. 6c). At the same time, we quantitated the frequencies of CD8 T cells within these same tumor-bearing kidneys from lean and DIO mice. Interestingly, while analysis of tumor-bearing kidneys from lean mice showed a significant increase in the frequency of CD8 T cells within the kidney tissue, this was not seen

in the tumor-bearing kidneys from DIO mice (Fig. 6d, e). The data in Fig. 6c–e also allowed us to determine the ratio of total numbers of CD8 T cell to MDSC in the kidney tissue. Ad5-TRAIL/CpG therapy in lean mice shifted the ratio heavily in favor of CD8 T cells, whereas the ratio of CD8 T cell/MDSC was nearly unchanged in Ad5-TRAIL/CpG-treated DIO mice compared to PBS-treated DIO mice (Fig. 6f). Finally, we examined the suppressive capacity of MDSC from lean and DIO mice directly ex vivo and after 3 h CpG stimulation. There was no significant difference in the ability of unstimulated and CpG-stimulated MDSC from DIO mice to suppress CD8 T-cell proliferation unlike that seen for MDSC from lean mice (Fig. 6g). Together, the data in Fig. 6 suggest that the increase in MDSC, as well as their resistance to CpG-mediated modulation, contributes to the ineffectiveness of Ad5-TRAIL/CpG therapy in DIO mice.

Discussion

With increasing investigation into the induction of MDSC by tumors and the mechanisms of suppression used by MDSC, a paradigm shift has taken place with regard to their acceptance as a means by which tumors evade antitumor immunity. Initially, the goal of cancer immunotherapy was simply to activate the host immune response to mount a robust antitumor response, but in recent years, it has become increasingly clear that effective cancer immunotherapy regimens must concomitantly modulate immunosuppressive cell populations. To this end, many studies have utilized combinations of chemotherapy and immunotherapy to modulate MDSC while inducing antitumor immunity, respectively. A complication of these combination therapies is the mounting evidence that chemotherapy can actually dampen the antitumor immune response, specifically when given prior to an immunotherapy, and that these effects can be long-lasting [9, 41]. The question then becomes, is there a combination therapy that can decrease immunosuppression while still stimulating a robust immune response? The data reported herein suggest that immunostimulatory CpG, which have been used extensively in the last 20 years as adjuvants in a number of infection and cancer settings [42], modulate the number and immunosuppressive function of MDSC in a mouse model of advanced RCC to allow for optimal generation of an antitumor immune response.

MDSC are present and promote tumor growth in humans with RCC and mouse models of RCC that use the renal adenocarcinoma cell line Renca. While MDSC depletion/modulation by a variety of therapies (e.g., sunitinib, 5-FU, and anti-Gr-1 mAb) can slow tumor progression, these therapies have not shown clear and consistent success in curing tumor-bearing animals (or humans) when given alone—especially in the cases of metastatic cancer [9, 16, 32]. These reports suggest that while depletion/modulation of MDSC is certainly beneficial, altering the quantity and quality of MDSC might not be enough to lead to complete tumor eradication. We have previously described the ability of Ad5-TRAIL/CpG therapy to clear primary orthotopic and metastatic RCC tumors in mice [20], and here, we have presented data to suggest that the mechanism by which Ad5-TRAIL/CpG therapy induces a potent antitumor response is through modulation of the number and function of MDSC. We have confirmed the increased presence of MDSC in Renca-bearing mice and have characterized the MDSC in this model. Both $Ly6G^+$ and $Ly6G^-$ MDSC accumulate systemically and locally during tumor challenge, and both subsets exhibit the canonical ability to suppress T-cell proliferation. Despite increases in immunosuppressive MDSC cells at the time of treatment, Ad5-TRAIL/CpG therapy modulates the number and function of these MDSC and induces a CD8 T-cell response responsible for tumor eradication in RCC-bearing mice.

Reports recently published by Zoglmeier et al. [43] and Shirota et al. [37] suggest that CpG-induced modulation of MDSC can occur via indirect and direct mechanisms, respectively. MDSC express TLR9, and direct stimulation by CpG leads to their differentiation into F4/80-expressing macrophages and loss of immunosuppressive function [37]. Murine plasmacytoid DC (pDC), Mϕ, B cells, and all myeloid DC subsets identified to date express TLR9 and respond to CpG [44]. pDC are primary producers of type I IFN after CpG stimulation, and the type I IFN produced by CpG-stimulated pDC can also induce MDSC maturation [43]. Our in vitro data also suggest the potential for direct CpG effects on the MDSC mobilized by Renca tumor growth, as the stimulation of purified MDSC from Renca-bearing mice with CpG underwent phenotypic change and demonstrated less suppressive capacity, much like the data from the Zoglmeier study. We also observed CpG-dependent alterations in vivo, but the data cannot define the extent to which these phenotypic changes were due to direct or indirect effects. Regardless of whether the CpG is acting directly or indirectly on the expanded MDSC within the tumor-bearing mice in our model, our data extend the previous findings to suggest that systemic alterations in physiology during comorbidities (in this case, obesity) can have profound effects on the mobilization of this immunosuppressive cell population and their sensitivity to immunostimulatory molecules.

When investigating MDSC, it is common to see the analysis of MDSC located in the spleen or blood from tumor-bearing mice or humans. These tissues are likely chosen because of convention and/or convenience (especially for humans), even when the tumor is located at a site that is not highly vascularized. Because we were investigating the influence of MDSC in the tumor tissue (where they presumably have the greatest effect on suppressing antitumor immunity), we felt it was essential to clearly and precisely

analyze those MDSC that were truly present within the tumor microenvironment of the tumor-bearing kidney compared to those that happened to be in the renal circulation at the time of tissue harvest. To our knowledge, this is the first report to utilize an intravascular staining technique that enabled the analysis of MDSC in a highly vascularized tumor-bearing organ before and after therapy. Utilizing this technique, we were able to determine changes in the ratio of CD8 T cells to MDSC within the same kidney tissue after therapy administration (Fig. 6f), which would not have been possible utilizing traditional approaches for MDSC analysis. Further, the ability to distinguish and assess differences in the phenotype and function of immune cells specifically within the kidney tissue versus the kidney vasculature (presumably in circulation) is possible.

Chronic inflammation is a characteristic of obesity, and the increased production of pro-inflammatory cytokines and adipokines during obesity can promote immune system dysfunction [39]. Despite the correlation between cancer, obesity, and cytokine-/adipokine-influenced inflammation, there are limited data regarding their relationship to MDSC presence and function. We previously showed that the Ad5-TRAIL/CpG therapy is ineffective in tumor-bearing DIO mice [22] and initially explored the contribution in alterations in DC function (as a result of obesity) to the lack of therapeutic efficacy. The data presented herein show the frequency of MDSC is higher in tumor-bearing obese mice than in lean mice, and the MDSC in the obese mice persist at a high frequency even after Ad5-TRAIL/CpG therapy. It remains to be determined whether the maintenance of elevated MDSC during obesity is due to intrinsic and/or environmental changes, as well as elucidating the functional mechanisms of MDSC from lean and DIO mice.

Obesity has become a critical health concern in the United States, as the majority of the adults are considered overweight or obese and the annual health care costs linked to obesity are >$100 billion (http://cdc.gov/nccdphp/dnpa/obesity/). Obese humans face an increased risk of cancer, including RCC [45]. The reasons for this are complex and multifactorial, but generalized immune suppression may contribute to these findings. In mice, obesity can be induced genetically or with a prolonged diet of HFF. DIO using HFF represents a slowly progressing, clinically relevant model characterized by alterations in adipokines and cytokines that induce systemic inflammation [46–48]. Studies using DIO mice have defined a number of alterations in leukocyte function [49–54]. There are data to suggest that the reduction in immune function is not associated with obesity, but rather due to the high-fat diet [55–57]. While it is possible that the high-fat diet (and not obesity) was behind the changes in the immune system response to Ad5-TRAIL/CpG therapy in the DIO mice used in our studies, there are two things that would suggest the high-fat diet was not the cause. First, in our model of DIO, some of the mice on HFF do not gain enough weight to be defined as obese based on our criteria [22]. We have in vitro data showing the HFF obese-resistant mice have immunological function similar to mice fed normal chow (data not shown). If the HFF diet, and not obesity itself, was the driving factor for the immune dysregulation in our DIO mice, the obese-resistant mice would have exhibited a similar phenotype. Second, many of the immunological defects seen in DIO mice have also been reported in genetically driven obesity (e.g., due to leptin or leptin receptor deficiency) [58–60]. Together, these data would suggest that the obese environment, and not the HFF diet, caused the immunoregulation evident in DIO mice.

In summary, the findings presented here suggest a heretofore unappreciated function of Ad5-TRAIL/CpG therapy. In addition to its previously described functions of inducing tumor cell death (via Ad5-TRAIL) and stimulating DC function (via CpG), the data herein suggest that the efficacy of Ad5-TRAIL/CpG therapy blocks the immunosuppressive effects of MDSC in the tumor microenvironment—both by decreasing MDSC frequency and modulating MDSC function.

Acknowledgments We thank the University of Iowa Gene Transfer Vector Core for the production of the Ad5-TRAIL vector. This work was supported by a University of Minnesota Doctoral Dissertation Fellowship (BR James), T90DE022732 from the National Institute of Dental & Craniofacial Research (KG Anderson), a Kidney Cancer Association Research Scholarship administered by the American Urological Association (EL Brincks), and the National Institutes of Health Grants AI084913 (D Masopust) and CA109446 (TS Griffith).

Conflict of interest B. James, K. Anderson, E. Brincks, T. Kucaba, L. Norian, D. Masopust, and T. Griffith declare that they have no conflict of interest.

References

1. Kusmartsev S, Gabrilovich DI (2006) Role of immature myeloid cells in mechanisms of immune evasion in cancer. Cancer Immunol Immunother 55:237–245. doi:10.1007/s00262-005-0048-z
2. Drake CG, Jaffee E, Pardoll DM (2006) Mechanisms of immune evasion by tumors. Adv Immunol 90:51–81. doi:10.1016/S0065-2776(06)90002-9
3. Mittal D, Gubin MM, Schreiber RD, Smyth MJ (2014) New insights into cancer immunoediting and its three component phases-elimination, equilibrium and escape. Curr Opin Immunol 27C:16–25. doi:10.1016/j.coi.2014.01.004
4. Ostrand-Rosenberg S (2010) Myeloid-derived suppressor cells: more mechanisms for inhibiting antitumor immunity. Cancer Immunol Immunother 59:1593–1600. doi:10.1007/s00262-010-0855-8
5. Ostrand-Rosenberg S, Sinha P, Beury DW, Clements VK (2012) Cross-talk between myeloid-derived suppressor cells (MDSC), macrophages, and dendritic cells enhances tumor-induced immune suppression. Sem Cancer Biol 22:275–281. doi:10.1016/j.semcancer.2012.01.011
6. Ko JS, Rayman P, Ireland J, Swaidani S, Li G, Bunting KD, Rini B, Finke JH, Cohen PA (2010) Direct and differential

suppression of myeloid-derived suppressor cell subsets by sunitinib is compartmentally constrained. Cancer Res 70:3526–3536. doi:10.1158/0008-5472.CAN-09-3278
7. Rodriguez PC, Ernstoff MS, Hernandez C, Atkins M, Zabaleta J, Sierra R, Ochoa AC (2009) Arginase I-producing myeloid-derived suppressor cells in renal cell carcinoma are a subpopulation of activated granulocytes. Cancer Res 69:1553–1560. doi:10.1158/0008-5472.CAN-08-1921
8. Ochoa AC, Zea AH, Hernandez C, Rodriguez PC (2007) Arginase, prostaglandins, and myeloid-derived suppressor cells in renal cell carcinoma. Clin Cancer Res 13:721s–726s. doi:10.1158/1078-0432.CCR-06-2197
9. Fridlender ZG, Sun J, Singhal S, Kapoor V, Cheng G, Suzuki E, Albelda SM (2010) Chemotherapy delivered after viral immunogene therapy augments antitumor efficacy via multiple immune-mediated mechanisms. Mol Ther 18:1947–1959. doi:10.1038/mt.2010.159
10. Kao J, Ko EC, Eisenstein S, Sikora AG, Fu S, Chen SH (2011) Targeting immune suppressing myeloid-derived suppressor cells in oncology. Crit Rev Oncol Hematol 77:12–19. doi:10.1016/j.critrevonc.2010.02.004
11. Ko JS, Zea AH, Rini BI, Ireland JL, Elson P, Cohen P, Golshayan A, Rayman PA, Wood L, Garcia J, Dreicer R, Bukowski R, Finke JH (2009) Sunitinib mediates reversal of myeloid-derived suppressor cell accumulation in renal cell carcinoma patients. Clin Cancer Res 15:2148–2157. doi:10.1158/1078-0432.CCR-08-1332
12. Najjar YG, Finke JH (2013) Clinical perspectives on targeting of myeloid derived suppressor cells in the treatment of cancer. Front Oncol 3:49. doi:10.3389/fonc.2013.00049
13. Xia S, Sha H, Yang L, Ji Y, Ostrand-Rosenberg S, Qi L (2011) Gr-1+ CD11b+ myeloid-derived suppressor cells suppress inflammation and promote insulin sensitivity in obesity. J Biol Chem 286:23591–23599. doi:10.1074/jbc.M111.237123
14. Matsuzaki J, Tsuji T, Chamoto K, Takeshima T, Sendo F, Nishimura T (2003) Successful elimination of memory-type CD8+ T cell subsets by the administration of anti-Gr-1 monoclonal antibody in vivo. Cell Immunol 224:98–105
15. Dalod M, Salazar-Mather TP, Malmgaard L, Lewis C, Asselin-Paturel C, Briere F, Trinchieri G, Biron CA (2002) Interferon alpha/beta and interleukin 12 responses to viral infections: pathways regulating dendritic cell cytokine expression in vivo. J Exp Med 195:517–528
16. Vincent J, Mignot G, Chalmin F, Ladoire S, Bruchard M, Chevriaux A, Martin F, Apetoh L, Rebe C, Ghiringhelli F (2010) 5-Fluorouracil selectively kills tumor-associated myeloid-derived suppressor cells resulting in enhanced T cell-dependent antitumor immunity. Cancer Res 70:3052–3061. doi:10.1158/0008-5472.CAN-09-3690
17. Mozaffari F, Lindemalm C, Choudhury A, Granstam-Bjorneklett H, Lekander M, Nilsson B, Ojutkangas ML, Osterborg A, Bergkvist L, Mellstedt H (2009) Systemic immune effects of adjuvant chemotherapy with 5-fluorouracil, epirubicin and cyclophosphamide and/or radiotherapy in breast cancer: a longitudinal study. Cancer Immunol Immunother 58:111–120. doi:10.1007/s00262-008-0530-5
18. Mozaffari F, Lindemalm C, Choudhury A, Granstam-Bjorneklett H, Helander I, Lekander M, Mikaelsson E, Nilsson B, Ojutkangas ML, Osterborg A, Bergkvist L, Mellstedt H (2007) NK-cell and T-cell functions in patients with breast cancer: effects of surgery and adjuvant chemo- and radio-therapy. Br J Cancer 97:105–111. doi:10.1038/sj.bjc.6603840
19. Kemp TJ, Kim J-S, Crist SA, Griffith TS (2003) Induction of necrotic tumor cell death by TRAIL/Apo-2L. Apoptosis 8:587–599
20. Norian LA, Kresowik TP, Rosevear HM, James BR, Rosean TR, Lightfoot AJ, Kucaba TA, Schwarz C, Weydert CJ, Henry MD, Griffith TS (2012) Eradication of metastatic renal cell carcinoma after adenovirus-encoded TNF-related apoptosis-inducing ligand (TRAIL)/CpG immunotherapy. PLoS One 7:e31085. doi:10.1371/journal.pone.0031085
21. Anderson KG, Mayer-Barber K, Sung H, Beura L, James BR, Taylor JJ, Qunaj L, Griffith TS, Vezys V, Barber DL, Masopust D (2014) Intravascular staining for discrimination of vascular and tissue leukocytes. Nat Protoc 9:209–222. doi:10.1038/nprot.2014.005
22. James BR, Tomanek-Chalkley A, Askeland EJ, Kucaba T, Griffith TS, Norian LA (2012) Diet-induced obesity alters dendritic cell function in the presence and absence of tumor growth. J Immunol 189:1311–1321. doi:10.4049/jimmunol.1100587
23. Hrushesky WJ, Murphy GP (1973) Investigation of a new renal tumor model. J Surg Res 15:327–336
24. VanOosten RL, Griffith TS (2007) Activation of tumor-specific CD8$^+$ T Cells after intratumoral Ad5-TRAIL/CpG oligodeoxynucleotide combination therapy. Cancer Res 67:11980–11990
25. James BR, Brincks EL, Kucaba TA, Boon L, Griffith TS (2014) Effective TRAIL-based immunotherapy requires both plasmacytoid and CD8a DC. Cancer Immunol Immunother 63:685–697
26. Hanson HL, Donermeyer DL, Ikeda H, White JM, Shankaran V, Old LJ, Shiku H, Schreiber RD, Allen PM (2000) Eradication of established tumors by CD8+ T cell adoptive immunotherapy. Immunity 13:265–276
27. Kusmartsev S, Eruslanov E, Kubler H, Tseng T, Sakai Y, Su Z, Kaliberov S, Heiser A, Rosser C, Dahm P, Siemann D, Vieweg J (2008) Oxidative stress regulates expression of VEGFR1 in myeloid cells: link to tumor-induced immune suppression in renal cell carcinoma. J Immunol 181:346–353
28. Rocha FG, Chaves KC, Chammas R, Peron JP, Rizzo LV, Schor N, Bellini MH (2010) Endostatin gene therapy enhances the efficacy of IL-2 in suppressing metastatic renal cell carcinoma in mice. Cancer Immunol Immunother 59:1357–1365. doi:10.1007/s00262-010-0865-6
29. Salup RR, Back TC, Wiltrout RH (1987) Successful treatment of advanced murine renal cell cancer by bicompartmental adoptive chemoimmunotherapy. J Immunol 138:641–647
30. Gabrilovich DI, Bronte V, Chen SH, Colombo MP, Ochoa A, Ostrand-Rosenberg S, Schreiber H (2007) The terminology issue for myeloid-derived suppressor cells. Cancer Res 67:425; author reply 426. doi:10.1158/0008-5472.CAN-06-3037
31. Youn JI, Nagaraj S, Collazo M, Gabrilovich DI (2008) Subsets of myeloid-derived suppressor cells in tumor-bearing mice. J Immunol 181:5791–5802
32. Movahedi K, Guilliams M, Van den Bossche J, Van den Bergh R, Gysemans C, Beschin A, De Baetselier P, Van Ginderachter JA (2008) Identification of discrete tumor-induced myeloid-derived suppressor cell subpopulations with distinct T cell-suppressive activity. Blood 111:4233–4244. doi:10.1182/blood-2007-07-099226
33. Kusmartsev S, Gabrilovich DI (2005) STAT1 signaling regulates tumor-associated macrophage-mediated T cell deletion. J Immunol 174:4880–4891
34. Greifenberg V, Ribechini E, Rossner S, Lutz MB (2009) Myeloid-derived suppressor cell activation by combined LPS and IFN-gamma treatment impairs DC development. Eur J Immunol 39:2865–2876. doi:10.1002/eji.200939486
35. Ueha S, Shand FH, Matsushima K (2011) Myeloid cell population dynamics in healthy and tumor-bearing mice. Int Immunopharmacol 11:783–788. doi:10.1016/j.intimp.2011.03.003
36. Messai Y, Noman MZ, Derouiche A, Kourda N, Akalay I, Hasmim M, Stasik I, Ben Jilani S, Chebil M, Caignard A, Azzarone B, Gati A, Ben Ammar Elgaaied A, Chouaib S (2010) Cytokeratin 18 expression pattern correlates with renal cell carcinoma progression: relationship with Snail. Int J Oncol 36:1145–1154

37. Shirota Y, Shirota H, Klinman DM (2012) Intratumoral injection of CpG oligonucleotides induces the differentiation and reduces the immunosuppressive activity of myeloid-derived suppressor cells. J Immunol 188:1592–1599. doi:10.4049/jimmunol.1101304
38. Bunt SK, Yang L, Sinha P, Clements VK, Leips J, Ostrand-Rosenberg S (2007) Reduced inflammation in the tumor microenvironment delays the accumulation of myeloid-derived suppressor cells and limits tumor progression. Cancer Res 67:10019–10026. doi:10.1158/0008-5472.CAN-07-2354
39. Ouchi N, Parker JL, Lugus JJ, Walsh K (2011) Adipokines in inflammation and metabolic disease. Nature Rev Immunol 11:85–97. doi:10.1038/nri2921
40. Okwan-Duodu D, Umpierrez GE, Brawley OW, Diaz R (2013) Obesity-driven inflammation and cancer risk: role of myeloid derived suppressor cells and alternately activated macrophages. Am J Cancer Res 3:21–33
41. Litterman AJ, Zellmer DM, Grinnen KL, Hunt MA, Dudek AZ, Salazar AM, Ohlfest JR (2013) Profound impairment of adaptive immune responses by alkylating chemotherapy. J Immunol 190:6259–6268. doi:10.4049/jimmunol.1203539
42. Krieg AM (2012) CpG still rocks! Update on an accidental drug. Nucleic Acid Ther 22:77–89. doi:10.1089/nat.2012.0340
43. Zoglmeier C, Bauer H, Norenberg D, Wedekind G, Bittner P, Sandholzer N, Rapp M, Anz D, Endres S, Bourquin C (2011) CpG blocks immunosuppression by myeloid-derived suppressor cells in tumor-bearing mice. Clin Cancer Res 17:1765–1775. doi:10.1158/1078-0432.CCR-10-2672
44. Suzuki K, Suda T, Naito T, Ide K, Chida K, Nakamura H (2005) Impaired toll-like receptor 9 expression in alveolar macrophages with no sensitivity to CpG DNA. Am J Respir Crit Care Med 171:707–713. doi:10.1164/rccm.200408-1078OC
45. Laber DA (2006) Risk factors, classification, and staging of renal cell cancer. Med Oncol 23:443–454. doi:10.1385/MO:23:4:443
46. Xu H, Barnes GT, Yang Q, Tan G, Yang D, Chou CJ, Sole J, Nichols A, Ross JS, Tartaglia LA, Chen H (2003) Chronic inflammation in fat plays a crucial role in the development of obesity-related insulin resistance. J Clin Invest 112:1821–1830. doi:10.1172/JCI19451
47. Lee IS, Shin G, Choue R (2010) Shifts in diet from high fat to high carbohydrate improved levels of adipokines and pro-inflammatory cytokines in mice fed a high-fat diet. Endocrine J 57:39–50
48. Fenton JI, Nunez NP, Yakar S, Perkins SN, Hord NG, Hursting SD (2009) Diet-induced adiposity alters the serum profile of inflammation in C57BL/6N mice as measured by antibody array. Diabetes Obes Metab 11:343–354. doi:10.1111/j.1463-1326.2008.00974.x
49. Karlsson EA, Sheridan PA, Beck MA (2010) Diet-induced obesity in mice reduces the maintenance of influenza-specific CD8+ memory T cells. J Nutr 140:1691–1697. doi:10.3945/jn.110.123653
50. Karlsson EA, Sheridan PA, Beck MA (2010) Diet-induced obesity impairs the T cell memory response to influenza virus infection. J Immunol 184:3127–3133. doi:10.4049/jimmunol.0903220
51. Kim CS, Lee SC, Kim YM, Kim BS, Choi HS, Kawada T, Kwon BS, Yu R (2008) Visceral fat accumulation induced by a high-fat diet causes the atrophy of mesenteric lymph nodes in obese mice. Obesity (Silver Spring) 16:1261–1269. doi:10.1038/oby.2008.55
52. Lumeng CN, DelProposto JB, Westcott DJ, Saltiel AR (2008) Phenotypic switching of adipose tissue macrophages with obesity is generated by spatiotemporal differences in macrophage subtypes. Diabetes 57:3239–3246. doi:10.2337/db08-0872
53. Smith AG, Sheridan PA, Tseng RJ, Sheridan JF, Beck MA (2009) Selective impairment in dendritic cell function and altered antigen-specific CD8+ T-cell responses in diet-induced obese mice infected with influenza virus. Immunology 126:268–279. doi:10.1111/j.1365-2567.2008.02895.x
54. Verwaerde C, Delanoye A, Macia L, Tailleux A, Wolowczuk I (2006) Influence of high-fat feeding on both naive and antigen-experienced T-cell immune response in DO10.11 mice. Scand J Immunol 64:457–466. doi:10.1111/j.1365-3083.2006.01791.x
55. Mito N, Kaburagi T, Yoshino H, Imai A, Sato K (2006) Oral-tolerance induction in diet-induced obese mice. Life Sci 79:1056–1061. doi:10.1016/j.lfs.2006.03.015
56. Cui J, Xiao Y, Shi YH, Wang B, Le GW (2012) Lipoic acid attenuates high-fat-diet-induced oxidative stress and B-cell-related immune depression. Nutrition 28:275–280. doi:10.1016/j.nut.2011.10.016
57. Miyazaki Y, Iwabuchi K, Iwata D, Miyazaki A, Kon Y, Niino M, Kikuchi S, Yanagawa Y, Kaer LV, Sasaki H, Onoe K (2008) Effect of high fat diet on NKT cell function and NKT cell-mediated regulation of Th1 responses. Scand J Immunol 67:230–237. doi:10.1111/j.1365-3083.2007.02062.x
58. Macia L, Delacre M, Abboud G, Ouk TS, Delanoye A, Verwaerde C, Saule P, Wolowczuk I (2006) Impairment of dendritic cell functionality and steady-state number in obese mice. J Immunol 177:5997–6006
59. Batra A, Okur B, Glauben R, Erben U, Ihbe J, Stroh T, Fedke I, Chang HD, Zeitz M, Siegmund B (2010) Leptin: a critical regulator of CD4+ T-cell polarization in vitro and in vivo. Endocrinology 151:56–62. doi:10.1210/en.2009-0565
60. Tian Z, Sun R, Wei H, Gao B (2002) Impaired natural killer (NK) cell activity in leptin receptor deficient mice: leptin as a critical regulator in NK cell development and activation. Biochem Biophys Res Commun 298:297–302